

A Deep Dive into the Impact of Solar Storms on LEO Satellite Networks

Eunju Kang
University of California, Irvine
USA
eunjuk2@uci.edu

Alagappan Ramanathan
University of California, Irvine
USA
alagappr@uci.edu

Sangeetha Abdu Jyothi
University of California, Irvine
USA
sangeetha.aj@uci.edu

Abstract

Low Earth Orbit (LEO) satellite networks are an important part of the global communication infrastructure today. Despite ongoing efforts to improve their resilience, they remain vulnerable to component damage and deorbiting under harsh space weather conditions. Prior work identified a modest but noticeable impact on LEO satellite network performance during solar storms, typically manifesting as an immediate rise in packet loss and a sustained increase in round-trip time (RTT). However, these studies offer only coarse-grained insights and do not capture the nuanced spatial and temporal patterns of disruption across the LEO network.

In this paper, we conduct a deep dive into the impact of solar storms on LEO satellite communications. By localizing the impact of increased atmospheric drag at the level of individual satellites and orbits, we reveal significant heterogeneity in how different parts of the network are affected. We find that the degree of performance degradation varies significantly across geographic regions, depending on satellite positioning during the storm. Specifically, we find that *(i)* not all satellite orbits are equally vulnerable, *(ii)* within a given orbit, certain satellites experience disproportionate impact depending on their position relative to geomagnetic conditions, and *(iii)* autonomous maneuvering of satellites might be a cause of the sustained increase in RTT. Our findings uncover previously overlooked patterns of vulnerability in LEO satellite constellations and highlight the need for more adaptive, region-aware mitigation strategies to address space weather-induced network disruptions.

1 Introduction

Low Earth Orbit (LEO) satellite constellations are rapidly transforming global connectivity. With their ability to provide low-latency, wide-area coverage, LEO networks have become foundational to applications ranging from consumer Internet access to disaster response and maritime communications. Major initiatives such as Starlink [28] and OneWeb [25] have already deployed thousands of satellites, with plans for tens of thousands more. As dependence on LEO-based communication grows, ensuring its robustness becomes increasingly critical.

A major threat to LEO satellite operations is space weather. Satellites are directly exposed to extreme space weather events, such as solar flares and Coronal Mass Ejections (CMEs) [17]. These events, driven by increased solar activity, can elevate atmospheric drag at orbital altitudes, stressing hardware systems and affecting satellite trajectories [6, 8–10, 14, 15, 19, 24]. While significant engineering efforts have gone into improving satellite resilience, operational data from recent storms reveal persistent vulnerabilities, including network performance degradation and, in extreme cases, satellite deorbiting [23].

Prior work has shown that solar storms can cause modest yet measurable degradation in communication performance, typically manifesting as increased packet loss and elevated Round-Trip Time (RTT) [27]. However, past work tends to view the LEO network in aggregate, offering only coarse-grained insights. They do not account for the complex spatial and temporal dynamics of how different satellites and regions are affected during a storm. This gap limits our ability to design targeted mitigation strategies and adaptive communication protocols.

In this paper, we present a fine-grained analysis of solar storm impacts on LEO satellite networks. Using real-world network measurement data from RIPE probes connected to the Starlink network (AS 14593) and publicly available satellite position information across four solar storms in 2024, we investigate how atmospheric drag from geomagnetic disturbances affects different parts of the LEO constellation, and in turn, network performance.

Our study reveals significant heterogeneity in the impact based on the time and location of the storm. *(i)* *Geographic variation:* There are variations in network performance degradation across regions in terms of the time of peak impact. *(ii)* *Orbital disparities:* Not all orbital planes experience the same level of disruption during a storm. The extent of impact depends on the orientation of the orbit with respect to the sun during storm impact. *(iii)* *Location-based variations:* We recognize three broad location-based categories for highly impacted satellites. We identify relatively large altitude changes for satellites at high latitudes, those over the South Atlantic Anomaly (SAA) region [7], and those facing the sun during the time of solar storm impact. Additionally, we also uncover patterns in highly affected satellites across consecutive storm days, showing the propagation of impact across neighboring satellites.

By uncovering spatial patterns of vulnerability, our work provides actionable insights to improve the robustness of LEO communication systems. We also discuss implications for adaptive routing and long-term constellation design in the face of increasing solar activity.

2 Background

We provide a brief overview of prior work on the analysis of satellite network performance during solar storms.

While several works [16, 18, 21, 22, 26] have evaluated LEO satellite performance under normal operational conditions, the analysis under solar storms is limited. Recent work [27] explores the impact of the May 2024 storm on the Starlink network, highlighting the immediate impact on loss and delayed but sustained impact on RTTs. Furthermore, CosmicDance [9] uses real-world measurements to investigate the impact of solar storms on satellite orbits.

However, both works stop short of linking orbital dynamics during solar storms with real-time network performance degradation.

Atmospheric drag [1] plays a critical role in satellite behavior, particularly during periods of heightened solar activity. Increased solar radiation heats the Earth's upper atmosphere, causing it to expand and increase in density at higher altitudes. This denser atmosphere results in greater drag on LEO satellites, which in turn leads to orbital decay, often observed as a loss of altitude. Satellites must frequently compensate for this decay through propulsion maneuvers to maintain operational altitudes and prevent premature re-entry.

3 Results

In this section, we present a detailed analysis of the impact of solar storms on LEO network performance, using fine-grained network measurements and satellite position data. We analyze the regional effects of solar storms on network performance and examine patterns among the most impacted satellites and orbits in the LEO constellation.

3.1 Experimental Setup

Our evaluation combines three complementary data sources to quantify and correlate the impacts of solar storms on Starlink's network performance and orbital dynamics.

Network Performance Measurement: We leverage 76 RIPE Atlas probes [4] connected to the Starlink autonomous system (AS 14593) to capture effects in the network layer. These probes conduct continuous ping measurements every four minutes to two target sets: all DNS root servers and seven terrestrial anchor probes located in Germany, Singapore, the US, and the Netherlands. Figure 1 shows the geographic distribution of active Starlink probes during the evaluation period.

Solar Storms: The Disturbance storm time index (Dst) [3] captures the intensity of geomagnetic disturbance, where more negative values indicate stronger storms. We focus on four major CME events from 2024 (Figure 2), selected based on their Dst index: May 11th superstorm (peak Dst of -406 nT at 02:00 UTC), August 12th storm (peak Dst of -188 nT at 16:00 UTC), October 8th storm (peak Dst of -148 nT at 07:00 UTC), and October 11th superstorm (peak Dst of -333 nT at 01:00 UTC).

Satellite Orbital Analysis: We use Two-Line Element set (TLE) data from Space-Track [5] to quantify altitude variations in Starlink satellites during storm periods. The TLE data provide precise orbital parameters, updated approximately every 10 hours on average, enabling the detection of atmospheric drag-induced altitude changes.

3.2 Regional Impact Analysis

We conduct a fine-grained evaluation of the correlation between a probe's geographic location and the severity of impact. We focus on RTT analysis since packet loss manifests as brief spikes that complicate regional comparison.

Regional Grouping of Probes: We partition probes into four regions based on geographic concentration: US West (130°W to 110°W longitude), US Central (100°W to 85°W), US East (85°W to

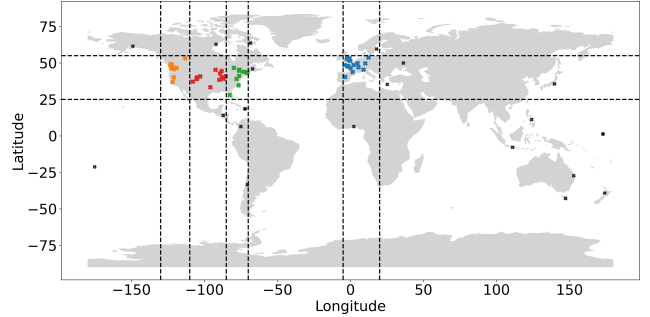


Figure 1: The locations of RIPE Atlas probes used in our analysis. The 76 probes span 23 countries and are connected to the Starlink AS (AS 14593). For regional analysis, we focus on probes in four regions: Europe (blue), US East (green), US Central (red), and US West (orange).

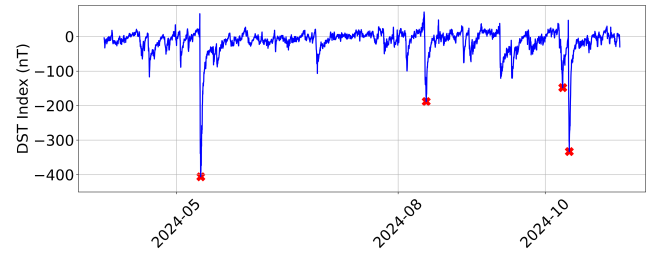


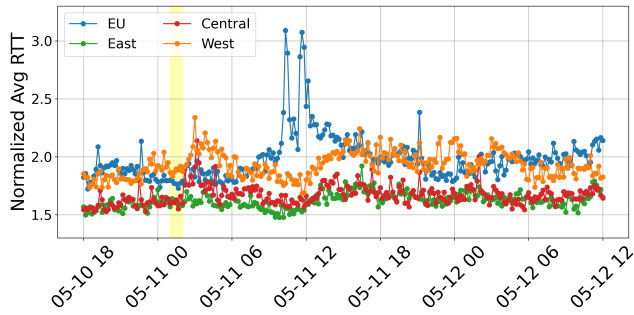
Figure 2: Geomagnetic activity in 2024 measured by Dst index. Red markers indicate the four major storms analyzed: May 11th (-406 nT), August 12th (-188 nT), October 8th (-148 nT), and October 11th (-333 nT).

70°W), and Europe (5°W to 20°E). All regions lie in the latitude range between 25°N and 55°N. Figure 1 shows the probe distribution across these regions. We exclude probes from the other regions due to small sample sizes.

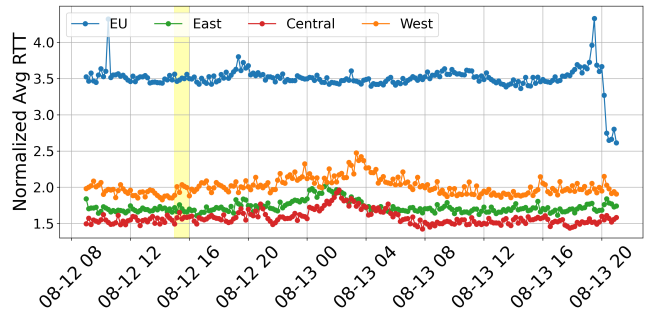
Methodology: For each storm, we calculate the normalized average RTT by dividing the observed RTT by the minimum RTT recorded for each pair of (measurement, probe) during the analysis time frame of 7 days (3 days before the storm, the day of the storm, and 3 days after the storm). This normalization enables cross-regional comparison. We aggregate measurements within 10-minute intervals to capture temporal dynamics while reducing noise.

Findings: Figure 3 presents normalized RTT across the four regions during the four storms. Consistent with previous findings [27], we observe a delayed increase in RTT that persists for several hours after the peak of the storm across all regions and storms. We do not find any systematic correlation between probe location and impact magnitude. However, we discover a striking temporal pattern in the peak values of RTT across regions. For instance, consider the October 8th storm (Figure 3c), peak RTTs occur at 18:00-19:00 UTC in Europe, followed by 00:00, 01:00, and 03:00 UTC in US East, US Central, and US West, respectively.

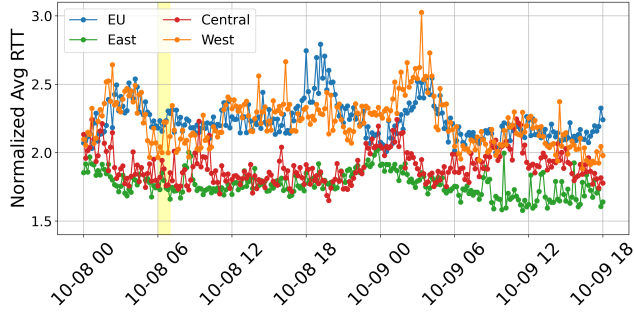
This temporal shift can be partially attributed to Starlink's orbital dynamics. Satellite orbits that are directly facing the storm over



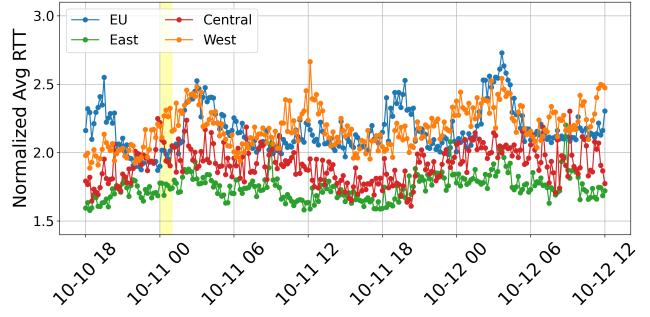
(a) May 11th super storm. The date and hour (UTC) are shown on the x-axis.



(b) August 12th storm. Peak RTTs following the storm occur at 19:00 UTC (Europe), 01:00 UTC (East), 02:00 UTC (Central), and 03:00 UTC (West).



(c) October 8th storm. Peak RTTs occur at 18:00-19:00 UTC (Europe), 00:00 UTC (East), 01:00 UTC (Central), and 03:00 UTC (West).



(d) October 11th super storm. The effects are less pronounced due to the cumulative effects of the Oct 8th storm.

Figure 3: Normalized RTT across four regions during four geomagnetic storms. Yellow bars indicate 1-hour range storm peaks (peak Dst times). There is a temporal progression in peak impact across regions, aligning with orbital shifts.

Europe subsequently pass over US regions as Earth rotates. While a satellite takes around 90 minutes to complete one orbit, the orbit's position will shift approximately 22.5° west relative to Earth during the same interval due to Earth's rotation. As a result, the orbital group above Europe will move over the US regions 5-8 hours later. This might partially explain the westward progression of the RTT peaks, although this interpretation is speculative.

Note that in the plots, some normalized RTT values are consistently above 1.0 since the normalization is with respect to the minimum across 7 days, while the visualization is over 2 days. Hence, the minimum may exist beyond the visualized interval. In addition, elevated values in certain regions reflect cumulative effects from preceding storms, since geomagnetic superstorms typically occur in clusters. The larger variance on October 11th is likely due to the cumulative effect from the preceding storm on October 8th.

3.3 Inter-Orbital Impact Analysis

Inspired by the time shift observed in peak network performance degradation across regions, we next investigate the orbit-level impact. We analyze altitude shifts of satellites per orbit using Two-Line Element (TLE) data, calculating the net magnitude of altitude changes in two consecutive TLEs for all satellites within each orbit. These altitude shifts reflect variations in atmospheric drag that correlate with network performance degradation.

Data processing: We leverage CosmicDance [9] to calculate the altitude of satellites from TLE data. There were ≈ 5800 Starlink satellites with TLE data during May 2024. However, to focus on the altitude change caused by the solar storm, we remove the satellites in the orbit-raising phase and those not in the planned orbital altitude, and analyze only the remaining 4708 satellites. To derive the position of the satellite at a specific time when TLE is not available, we use the SGP4 orbit propagator [11] to propagate the satellite position from the most recent TLE ephemeris. We group satellites by inclination, altitude, and right ascension of the ascending node (RAAN) to identify those having the same orbital path.

Patterns in Orbital Impact: Figure 4 presents box plots of altitude changes of the satellite across orbits at three inclinations (43°, 53°, and 70°) during the May 2024 superstorm peak (May 11th). Detailed plots including the fourth inclination of 97.6° (Figure 9) and corresponding plots from a non-storm period for comparison (Figure 10) are given in the Appendix. We calculate the change in altitude between consecutive TLE data on May 11th, averaging the values if multiple TLEs are available for the day. This altitude difference reflects both solar storm-induced decay and human-controlled orbital adjustments. We observe significant variations in the severity of impact across orbits within the same inclination, with certain orbits experiencing substantially higher altitude changes than others.

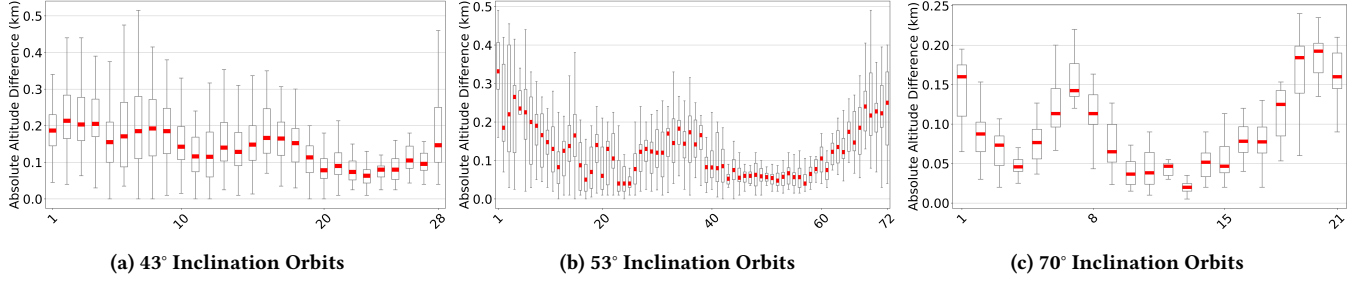


Figure 4: Altitude changes across orbital groups at three inclinations (43° , 53° , and 70°) during the May 2024 superstorm peak. Box plots show significant variation within inclinations and distinctive "W" patterns across orbits, indicating a systematic impact based on orbit orientation relative to solar storm direction. Higher-resolution images for four orbital inclinations (43° , 53° , 70° , and 97.6°) during the storm period are provided in Figure 9, with corresponding plots from a non-storm period included for comparison in Figure 10 in the Appendix.

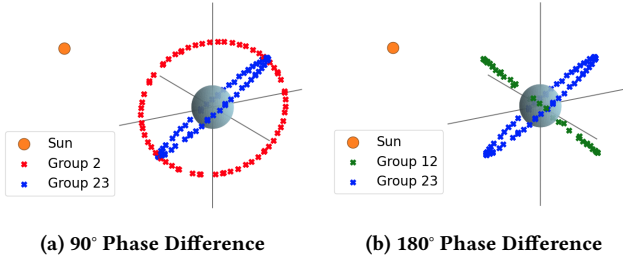


Figure 5: Orbit positions at 43° inclination during May 2024 superstorm. (a) The most (group 2) and the least impacted orbits (group 23) have a phase difference of 90° . (b) Group 12 and group 23 have $\approx 180^\circ$ of phase difference. Note that the sizes of the Sun, the Earth, and the orbits are not to scale, but their relative orientations are accurate.

The data reveals a distinctive "W" pattern in the box plots across all inclinations, indicating systematic variation in orbital impact based on orbit positioning. Orbit groups with the highest altitude changes contain satellites positioned to be closer to the Sun, experiencing solar radiation flux directly during the storm. Conversely, orbit groups with minimal impact had more satellites positioned farther away from the Sun.

Phase Relationship Analysis: To validate the hypothesis that orbital orientation with respect to the sun influences the extent of impact, we examine phase relationships between high-impacted and low-impacted orbits during the peak of the May 2024 superstorm. Note that the longitude-based phase difference between adjacent orbits depends on the number of orbits at each inclination. For example, at 53° , there are 72 orbits, leading to a phase shift between adjacent orbits of $360/72 = 5^\circ$.

In Figure 4, analyzing the mean absolute altitude change across various orbits at each inclination, we find consistent phase shifts of $80 - 100^\circ$ or $260 - 280^\circ$ (equivalent to -80° to -100°) between orbits experiencing maximum and minimum altitude changes. For instance, orbit group 2 and group 23 at 43° inclination, with the maximum altitude change and minimum altitude change, respectively, exhibit a 90° phase shift. Orbit group 1 and group 52, with maximum and minimum altitude change, respectively, at a 53° inclination, have around a 260° phase shift, which is equivalent to -100° . This $\approx 90^\circ$ phase separation between the most and least impacted orbits across

all inclinations confirms that orbital impact severity correlates with orbital orientation relative to incoming solar radiation.

Figure 5a shows positions for the most and least impacted orbits at 43° inclination during the May 2024 superstorm. The most affected group 2 has more satellites facing the sun, while the least affected group 23 is oriented $\approx 90^\circ$ from it. Additionally, in Figure 4, we observe variations in the extent of dips on the two halves of the "W" pattern. This can also be explained based on the orientation of the orbital plane with respect to the Sun. Figure 5b shows that orbit group 12, with $\approx 180^\circ$ phase difference with respect to group 23, has nearly half of the satellites oriented toward the Sun. Hence, the dip around group 12 is less pronounced than that around group 23 in the "W" pattern. Thus, orbital analysis provides evidence that solar storm impacts on LEO satellites depend critically on satellite orientation relative to the solar flux direction.

3.4 Geospatial Impact Analysis

While our previous analysis demonstrates differences across orbital groups, we next delve deeper to examine the geolocation of the most affected satellites during the storm. We again focus on the May 2024 superstorm. To identify satellites that experienced significant altitude changes at each inclination, we establish our impact threshold as the 95th percentile of average altitude changes observed on the day of the peak storm (May 11th). We identify the altitude change threshold for the 95th percentile as 0.325 km, the 97th percentile as 0.367 km, and the 99th percentile as 0.45 km.

Figure 6 shows the positions of the most severely impacted satellites across all inclinations on May 11th at approximately 02:00 UTC, coinciding with the peak Dst index.

Spatial Impact Patterns: Our analysis reveals interesting patterns in the spatial distribution of impacted satellites, which can be broadly classified into three distinct groups. First, most of the severely impacted satellites are positioned at higher latitudes, consistent with the enhanced atmospheric drag in polar regions that occurs during geomagnetic storms. Second, we observe a significant impact over the South Atlantic region, where the South Atlantic Anomaly (SAA) [2, 7] is known to create enhanced exposure due to a weakened Earth's magnetic field. The third subset of highly impacted satellites is primarily located over regions that experienced daytime during the storm's peak Dst at 2:00 am UTC (notably

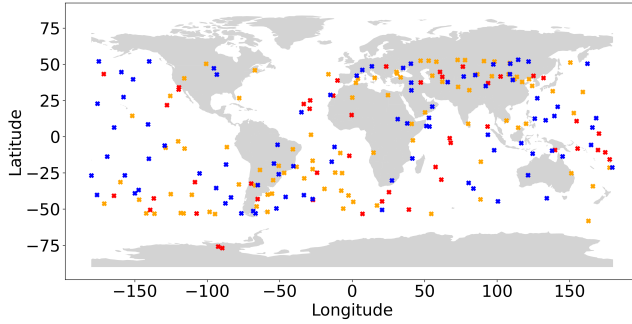


Figure 6: Spatial distribution of most impacted satellites at peak Dst during May 2024 superstorm. Impact severity shown by color: red (>99th percentile), orange (97-99th percentile), blue (95-97th percentile).

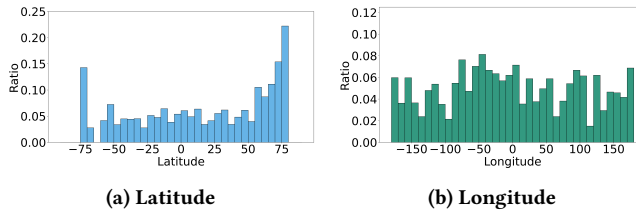


Figure 7: The fraction of highly impacted satellites across latitudes and longitudes during the August 2024 event. We observe a higher impact probability at higher latitudes. Furthermore, there is a higher impact on the region experiencing daytime during peak Dst.

Asia and the Pacific), suggesting enhanced atmospheric drag on the sun-facing side of Earth.

To validate our hypothesis regarding the categories, we further analyze the August 12th 2024 storm. This secondary case study demonstrates the generalizability of our findings across different storm events and examines patterns during a storm with relatively lower Dst magnitude compared to the May 2024 superstorm. Figures 7a and 7b present histogram analyses showing the fraction of highly impacted satellites among total satellites across latitudes and longitudes for the August 2024 event. Again, we observe that satellites at higher latitudes have significantly higher probabilities of being impacted by the storm. Additionally, it reveals a higher distribution during the daytime at the storm’s peak Dst, at 16:00 UTC, between 0° and -50° longitudes.

Clustered Pattern Across Multiple Days: While Figure 4 relies on TLE data from May 11th, a similar pattern is observed on May 12th, but with a different set of highly impacted satellites. Among the 236 satellites that are over the 95th percentile of altitude change on May 11th, only 30 satellites were also present in the highly impacted subset on May 12th. Interestingly, Figure 8 shows that the most impacted satellites across the two days, even when they are distinct, are positioned near each other. Thus, we observe that significant altitude changes propagate within and across orbits, affecting the neighboring satellites. We attribute this to the self-driving nature of LEO constellations, which perform automatic orbital maneuvers to calibrate satellite orbits and avoid collisions [20].

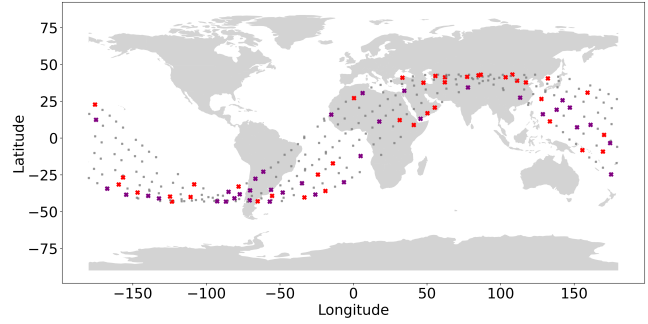


Figure 8: Position of satellites in groups 2 to 7 at inclination 43° at the Dst peak of May 2024 superstorm. Highly impacted satellites on May 11th marked in red, and high-impacted satellites on May 12th marked in purple.

4 Discussion

In this section, we discuss the implications of our findings on network design and resilience of LEO constellations.

Leveraging Predictability of Impact: Our findings demonstrate that satellites at high latitudes and those with direct solar exposure during storm peaks experience the most significant orbital decay, corroborating previous thermosphere ionosphere coupled simulations [12]. This predictability presents critical opportunities for enhancing network resilience through proactive management strategies.

Operators can implement preemptive network adaptations by integrating solar storm forecasts with our identified vulnerability patterns. Networks can dynamically reconfigure topologies, preposition backup communication paths through less-vulnerable satellites, and implement priority-based handover mechanisms that favor satellites likely to be in low-impact orbits. By predicting when and where satellites are likely to experience orbital degradation, networks can dynamically adapt routing protocols and create resilience zones by identifying satellite clusters likely to maintain stable performance during storms.

However, not all satellites traversing high-risk regions experience uniform altitude degradation. This variability is due to highly localized atmospheric density deviations and satellite-specific factors. This heterogeneity necessitates the development of probabilistic impact models that capture the stochastic nature of drag effects, enabling networks to make risk-aware routing decisions that balance performance optimization with reliability guarantees during space weather events.

The Propagation of Impact across Satellites: Our analysis reveals that different sets of satellites experience the most severe impacts across consecutive storm days, with only 30 out of 236 highly impacted satellites on May 11th remaining in the high-impact category on May 12th. While atmospheric density pockets could theoretically affect multiple satellites across days, the observed pattern of neighboring satellites being sequentially impacted suggests a different cause. We attribute this clustered propagation primarily to the self-driving nature of LEO constellations. Starlink employs a proprietary onboard autonomous control system to manage continuous orbit maintenance, collision avoidance, and inter-shell maneuvers. However, excessive or unnecessary maneuvers can lead to network

topology instability and performance degradation [20]. Analysis of TLE data reveals that when satellites experience altitude loss due to increased atmospheric drag, Starlink responds by temporarily raising the affected satellites above their nominal altitude. These satellites typically return to their original altitude within 1–2 days. This corrective action triggers a cascading effect, with orbital adjustments propagating across neighboring satellites in both spatial and temporal dimensions. Full stabilization of the orbit often takes 3–4 days. These dynamic adjustments can disrupt satellite links and routing paths, contributing to performance issues such as a sustained increase in round-trip time (RTT).

This finding raises fundamental questions about the suitability of today's autonomous constellation management during extreme space weather events. The self-driving algorithms, optimized for normal operations, may inadvertently amplify storm impacts by triggering chains of orbital adjustments. Network operators should investigate implementing storm-aware autonomous control modes that temporarily modify or disable certain self-driving behaviors during severe geomagnetic disturbances and introduce collective decision-making algorithms that consider space weather conditions when planning constellation-wide maneuvers.

A Real-time Monitoring Framework: A monitoring framework that compares predicted solar storm impact models against observed network performance metrics can enable the iterative refinement of probabilistic impact models in real time, in turn facilitating network adaptations. For example, such a monitoring system could provide early warning capabilities by detecting initial impacts in eastern regions before they propagate westward. This real-time validation loop would improve the accuracy of the 3-day forecast window typically available for solar storm predictions, allowing operators to make more informed decisions about preemptive network reconfigurations and resource allocation.

Limitations: Our analysis is constrained by the sparsity of available data sources. The satellite TLE data, with an average gap of 10 hours between reported positions, makes it difficult to determine the precise timing of satellite decay. Similarly, latency analysis is limited by the coarse resolution of ping measurements, taken every 4 minutes, which fail to capture short-term variations in loss and latency. Additionally, the sparse distribution of measurement probes at lower latitudes results in reduced data coverage in those regions.

The opaque nature of the Starlink system further constrains our analysis. Although RIPE Atlas measurements provide the geographic coordinates of probes, they do not reveal which satellite is serving a given probe at any point in time. Additionally, the lack of traceroute support within the Starlink network prevents us from identifying the satellite hops involved along a given path.

The observed impact of solar storms on satellite performance is also highly non-uniform. While a higher concentration of affected satellites appears at higher latitudes, not all satellites in these regions are impacted. Even in the most affected regions, no more than 20% of satellites experienced significant altitude changes. This uneven impact is likely due to local variations in atmospheric conditions along individual satellite paths. These findings underscore the need for a more detailed analysis to gain a deeper understanding of

the fine-grained dynamics of satellite behavior under solar storm conditions.

5 Conclusion

In this paper, we present a fine-grained analysis of the impact of solar storms on LEO networks by correlating real-world network performance data with satellite orbital dynamics across multiple storm events. Our study revealed significant spatial, temporal, and orbital heterogeneity in how solar activity impacts LEO network performance, highlighting vulnerable satellite regions, including high latitudes, sun-facing orbits, and the South Atlantic Anomaly. Future work should explore the design of adaptive network solutions as well as cross-layer control loops that integrate atmospheric drag forecasts, real-time RTT feedback, and autonomous satellite maneuver planning to build next-generation resilient satellite networks. While this study focuses on Starlink—the largest LEO constellation currently in operation—our methodology can be extended to analyze other systems such as OneWeb [25] and Kuiper [13].

References

- [1] [n. d.]. Satellite Drag | NOAA / NWS Space Weather Prediction Center. <https://www.swpc.noaa.gov/impacts/satellite-drag>.
- [2] [n. d.]. South Atlantic Anomaly - Wikipedia. https://en.wikipedia.org/wiki/South_Atlantic_Anomaly.
- [3] 2025. Real-time (Quicklook) Dst Index Monthly Plot and Table. https://wdc.kugi.kyoto-u.ac.jp/dst_realtime/index.html.
- [4] 2025. RIPE Atlas (Starlink Probes). <https://atlas.ripe.net/probes/public?search=14593>.
- [5] 2025. Space-Track.org. <https://www.space-track.org/>.
- [6] JH Allen. 1993. Solar-terrestrial activity affecting systems in space and on Earth. *Solar-Terrestrial predictions* (1993), 75–107.
- [7] PC Anderson, FJ Rich, and Stanislav Borisov. 2018. Mapping the South Atlantic Anomaly continuously over 27 years. *Journal of Atmospheric and Solar-Terrestrial Physics* 177 (2018), 237–246.
- [8] Daniel N Baker. 1984. *Effects of the solar-terrestrial environment on satellite operations*. Technical Report. Los Alamos National Lab.(LANL), Los Alamos, NM (United States).
- [9] Suvam Basak, Amitangshu Pal, and Debopam Bhattacharjee. 2024. CosmicDance: Measuring Low Earth Orbital Shifts due to Solar Radiations. In *Proceedings of the 2024 ACM on Internet Measurement Conference* (Madrid, Spain) (IMC '24). Association for Computing Machinery, New York, NY, USA, 19–28. <https://doi.org/10.1145/3646547.3689024>
- [10] LI Dorman, AV Belov, EA Eroshenko, LI Gromova, N Iucci, AE Levitin, M Parisi, NG Ptitsyna, LA Pustil'nik, MI Tyasto, et al. 2005. Different space weather effects in anomalies of the high and low orbital satellites. *Advances in Space Research* 36, 12 (2005), 2530–2536.
- [11] Ronald L. Roehrich Felix R. Hoots. 1980. *Models for Propagation of NORAD Element Sets*. Technical Report. Aerospace Defense Command Peterson AFB CO Office of Astrodynamics.
- [12] T. J. Fuller-Rowell, M. V. Codrescu, R. J. Moffett, and S. Quegan. 1994. Response of the thermosphere and ionosphere to geomagnetic storms. *Journal of Geophysical Research: Space Physics* 99, A3 (1994), 3893–3914. <https://doi.org/10.1029/93JA02015>
- [13] Caleb Henry. 2019. Amazon planning 3,236-satellite constellation for internet connectivity. <https://bit.ly/3qdAywU>.
- [14] RB Horne, SA Glauert, M. J. Meredith, D Boscher, V Maget, D Heynderickx, and D Pitchford. 2013. Space weather impacts on satellites and forecasting the Earth's electron radiation belts with SPACECAST. *Space Weather* 11, 4 (2013), 169–186.
- [15] N Iucci, AE Levitin, AV Belov, EA Eroshenko, NG Ptitsyna, G Villoresi, GV Chizhennkov, LI Dorman, LI Gromova, M Parisi, et al. 2005. Space weather conditions and spacecraft anomalies in different orbits. *Space weather* 3, 1 (2005).
- [16] L Izhikevich, M Tran, K Izhikevich, G Akiwate, and Z Durumeric. 2024. Democratizing LEO Satellite Network Measurement. *Proceedings of the ACM on Measurement and Analysis of Computing Systems* 8, 1 (2024), 1–26.
- [17] Sangeetha Abdu Jyothi. 2021. Solar Superstorms: Planning for an Internet Apocalypse. In *Proceedings of the 2021 ACM SIGCOMM 2021 Conference*. 692–704.
- [18] MM Kassem, A Raman, D Perino, and N Sastry. 2022. A browser-side view of starlink connectivity. In *Proceedings of the 22nd ACM Internet Measurement Conference*. 1–12.

Conference. 151–158.

[19] HC Koons and JF Fennell. 2006. Space weather effects on communications satellites. *URSI Radio Science Bulletin* 2006, 316 (2006), 27–41.

[20] Yuanjie Li, Hewu Li, Wei Liu, Lixin Liu, Wei Zhao, Yimei Chen, Jianping Wu, Qian Wu, Jun Liu, Zeqi Lai, and Han Qiu. 2023. A Networking Perspective on Starlink’s Self-Driving LEO Mega-Constellation. In *Proceedings of the 29th Annual International Conference on Mobile Computing and Networking* (Madrid, Spain) (ACM MobiCom ’23). Association for Computing Machinery, New York, NY, USA, Article 17, 16 pages. <https://doi.org/10.1145/3570361.3592519>

[21] S Ma, YC Chou, H Zhao, L Chen, X Ma, and J Liu. 2023. Network characteristics of LEO satellite constellations: A Starlink-based measurement from end users. In *IEEE INFOCOM 2023-IEEE Conference on Computer Communications*. IEEE, 1–10.

[22] F Michel, M Trevisan, D Giordano, and O Bonaventure. 2022. A first look at starlink performance. In *Proceedings of the 22nd ACM Internet Measurement Conference*. 130–136.

[23] R Miteva, SW Samwel, and S Tkatchova. 2023. Space Weather Effects on Satellites. *Astronomy* 2, 3 (2023), 165–179. <https://doi.org/10.3390/astronomy2030012>

[24] Sten Odenwald, James Green, and William Taylor. 2006. Forecasting the impact of an 1859-calibre superstorm on satellite resources. *Advances in Space Research* 38, 2 (2006), 280–297.

[25] OneWeb. 2023. OneWeb. <https://oneweb.net/>.

[26] A Raman, M Varvello, H Chang, N Sastry, and Y Zaki. 2023. Dissecting the performance of satellite network operators. *Proceedings of the ACM on Networking* 1, CoNEXT3 (2023), 1–25.

[27] Alagappan Ramanathan and Sangeetha Abdu Jyothi. 2024. Weathering a Solar Superstorm: Starlink Performance during the May 2024 Storm. In *Proceedings of the 2nd International Workshop on LEO Networking and Communication* (Washington, DC, USA) (LEO-NET ’24). Association for Computing Machinery, New York, NY, USA, 31–36. <https://doi.org/10.1145/3697253.3697270>

[28] SpaceX. 2023. Starlink. <https://www.starlink.com>.

A Appendix

Figure 9 presents box plots of altitude changes of the satellite across orbits at three inclinations (43° , 53° , 70° , and 97.6°) during the May 2024 superstorm peak (May 11th). We observe the distinctive “W” pattern across all inclinations. Figure 10 shows the altitude changes during a quiet period on April 11th and serves as the baseline for comparing storm and non-storm periods. The baseline period in Figure 10 has nearly uniform changes across orbit groups, while the characteristic “W” pattern in Figure 9 reflects the impact of the solar storm during the storm period.

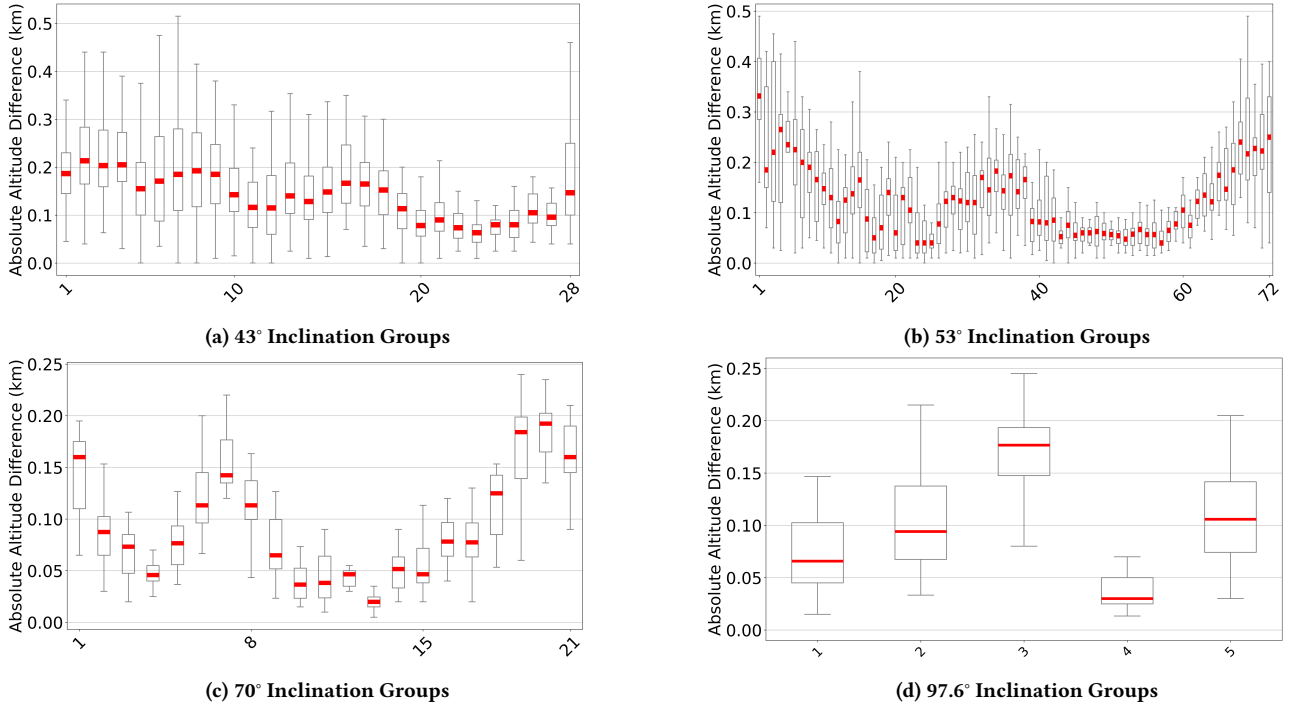


Figure 9: Altitude changes across orbital groups at four inclinations (43° , 53° , 70° , and 97.6°) during the May 2024 superstorm peak. Box plots show significant variation within inclinations and distinctive "W" patterns indicating systematic impact based on satellite orientation relative to solar storm direction.

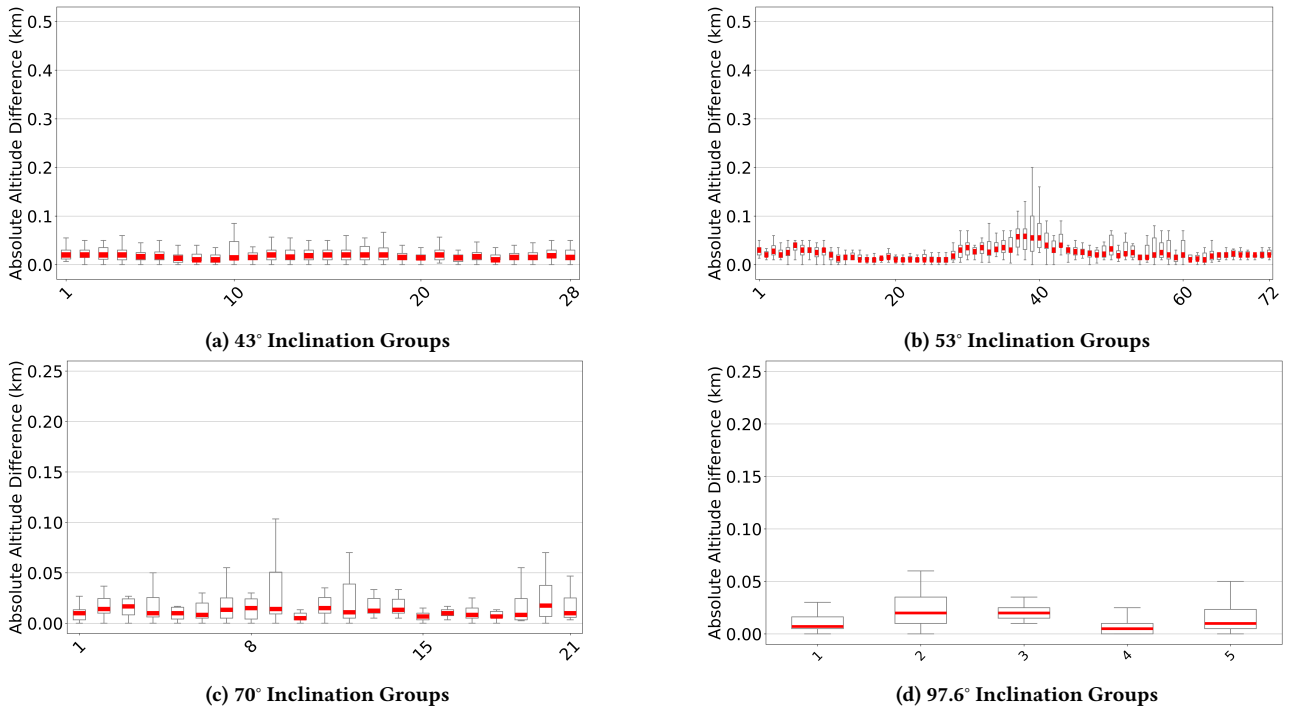


Figure 10: Altitude changes across orbital groups at four inclinations (43° , 53° , 70° , and 97.6°) during a quiet period (April 11th). The altitude changes are minimal and nearly uniform across all orbits. The y-axis of the plot is set to the same range as Figure 9 to enable visual comparison.